# A numerical Study on Impact and Compression after Impact Behaviour of Variable Angle Tow Laminates

Thi D. Dang[1] and Stephen R. Hallett[2]

*Advanced Composite Centre for Innovation and Science (ACCIS), University of Bristol,*

*Queen's Building, University Walk, BS8 1TR, UK*

Recent developments of variable angled tow (VAT) technology have indicated that variable stiffness composite laminates offer a strong potential for structural tailoring. However, the design complexity requires use of numerical analysis and novel techniques for this type of structural composites. This paper addresses the problem of the impact and compression after impact (CAI) behavior prediction of variable stiffness composite laminates with emphasis on the effect of the interaction between fibre orientations, matrix-cracks and delaminations. An explicit finite element analysis using bilinear cohesive law-based interface elements and cohesive contacts is employed for the investigation. Examples are presented to illustrate the effectiveness of the current models for predicting the extent of impact damage and subsequent compression strength. The current study has improved the understanding of interactions between matrix-cracks and delaminations to clarify open questions on delamination initiation and how matrix cracks and fibre orientations interact.

***Keywords*: VAT laminate, Delamination, matrix-crack, Impact behavior, CAI behavior, crack propagation, fibre orientation**

## 1. Introduction

In general there is demand from airlines that a new aircraft shows at least a 20% improvement in direct operating costs [1]. Although, a number of system-level improvements can lead to such a reduction in the direct operating costs, the aircraft industry often considers reducing the structural weight of the aircraft as one of the main options. NASA researchers [2] are expecting to reduce the weight of the fuselage structure by 25%, and are thus continuously looking at the means that will help it accomplish this goal.

Corresponding author.

[1] *E-mail address*: aextd@bristol.ac.uk (Thi Dang)
[2] *E-mail address*: stephen.hallett@bristol.ac.uk (Stephen Hallett)

With the increasing trend toward the use of composite materials for primary structure, researchers [2] are also looking at ways to tailor the direction and placement of fibre laminates. This can be achieved by steering the individual fiber tows to make curvilinear fiber paths and thus control the distribution of material to better suit the local load requirements. The recent manufacturing developments [3] in Variable Angle Tow (VAT) technology (where stiff carbon fibres are steered along curves to maximize structural performance) seem to meet the expectation of the aircraft industry. Other work at the University of Bristol [4-6] made a preliminary assessment of the manufacturability of the embroidery-based VAT process. This produced flat, low voidage, constant thickness, and high volume fraction VAT panels with high resistance to buckling as well as improved stiffness in deeper post-buckling. The original motivation for development of this technology [7-9] was that the response of fibre-reinforced laminates could be significantly altered by allowing the fibre orientation angle to vary spatially throughout the structure. Since the fibre orientation defines the stiffness properties of laminates, such structures are also termed *variable-stiffness composite panels*. The potential of VAT laminates opens a new branch of research in laminated composite materials; the design complexity requires use of numerical analysis and novel approaches to tackle problems for this type of structural composite laminates. As well as stiffness and buckling, damage resistance and tolerance are extremely important design drivers in aerospace structures. In this paper VAT laminates, which can bring advantages in terms of tailored stiffness and buckling resistance, are assessed through numerical analysis, for their response to impact and damage.

Structural composites display a wide variety of failure mechanisms as a result of their complex structure and manufacturing processes, which include fibre failure, fiber matrix debonding, matrix cracking, buckling and delamination. Delamination, that is, the debonding between adjacent laminate, is the most significant single failure mode in laminated composites since it significantly reduces the strength of the laminate. The greatest reduction is that of the compressive strength which may be up to 40–60% of that of an undamaged structure [10-11]. Delaminations are often induced by different types of impacts, of which low-energy impact is considered the most dangerous, because it is very difficult to detect in a routine visual inspection [12]. Therefore, the study of low-energy impact and compression after impact (CAI) behaviour of laminated composites is one of the most important problems in the design of composite structures. For laminated composites under low-velocity impacts, damage starts with the creation of a matrix crack. In thin laminates, a tensile crack in the bottom ply, perpendicular the plane of the laminate,

is often created by the flexural loading. For thick laminates, cracks appear near the top of the laminate, created by the local contact and shear stresses and are inclined relative to the plane of the laminate. Matrix cracks do not significantly contribute to the reduction in residual properties of the laminate. However, it is often argued that the damage evolution is initiated by matrix cracks which then induce delaminations at ply interfaces [13]. Therefore, a clear understanding of the interaction between matrix cracks and delaminations can help to understand damage initiation and evolution in composite structures. In the past, researchers have studied the effect of the interaction between matrix cracks and delamination in quasi-isotropic and straight fibre laminates, Lammerant and Verpoest [14] used a finite element analysis to investigate the initiation of delaminations at matrix cracks and the interaction of delaminations with matrix cracks using the energy criteria. Salpekar et al. [15] considered delamination growing at the intersection of a matrix crack and a free edge in an angle ply laminate using the virtual crack closure technique. An interface element model was used by Moura and Goncalves [16] with three dimensional solid elements to simulate the onset and growth of the bending crack and delamination. Ladeveze et al. [17] took into account of the effect of matrix cracking on delamination by modifying the respective damage parameters in their model in which the matrix cracking is considered as distributed throughout the continuum. Hallett et al [18] made an investigation during testing and examination of the failed test specimens of a flat quasi-isotropic laminate in tension that showed there was a strong influence of matrix cracking and delamination and modelled the interaction between them with interface elements. On the damage analysis of curvilinear fibre laminates, Lopes, Gurdal and Camanho [19] carried out first-ply failure analyses on variable-stiffness panels, optimised for buckling, by using the continuum damage mechanics-based failure model. Analyses were extended into the postbuckling progressive damage behaviour and final structural failure [20] due to accumulation of fibre and matrix damage. However, only failure modes at ply-level were considered. Failure modes of delamination at interfaces and the interaction between matrix cracks and delamination, which have shown to be important, were not addressed.

The motivation of the current paper is to study the impact and compression after impact (CAI) behaviour of VAT laminates with emphasis on the investigation of the interaction between fibre orientations and matrix-cracks and delaminations. For this purpose, an explicit finite element analysis using bilinear cohesive law-based interface elements and cohesive contacts in Abaqus/Explicit [21] is performed to

investigate the impact and CAI behaviour of VAT laminates with delamination and crack growth. Here interface elements are used to predict the onset and propagation of delamination at interfaces, while cohesive contacts are used to predict the onset and propagation of matrix cracks. Cohesive contact is a surface-based cohesive interaction defined in the surface-based cohesive behaviour framework of Abaqus/Explicit [21]. Its features are very similar to cohesive elements. Cohesive elements have been used to model the delamination since it is easier with this feature to transfer failed regions from the impact to CAI models. For the matrix cracks it is more appropriate to use the cohesive contact formulation since zero thickness is required and the contact formulation is easier to insert into the model in this case. Cohesive law-based interface elements are used in the paper for delamination prediction, because they have a number of advantages over other modeling approaches, such as the capacity to investigate both initiation and growth of damage, incorporating both strength and fracture based criteria [22-26]. Another added advantage is that the use of interface elements does not require an assumption of initial damage size or propagation direction. The potential for a single matrix crack to occur in the bottom ply of the laminates under investigation is included though insertion of duplicate nodes and cohesive contact. Its path is assumed to follow the fibre orientation. Also, experimental studies [13] consistently report that delaminations occur only at interfaces between plies with different fiber orientations. Thus, interface elements will be introduced only at the interface between them.

Two models were built for predicting the behaviour of VAT composite laminates with consideration of delamination and crack growth. Firstly, an impact model is developed to predict the damage induced by low-velocity impacts. Secondly, a compression after impact (CAI) model is presented to predict the compressive behaviour of the delaminated VAT laminate. The impact and CAI simulations are also performed for straight fibre laminates for comparison. In the CAI model of straight fibre laminates; one model has only delaminations while the other has both delaminations and a matrix crack to investigate the effect of matrix crack on delamination propagation and deformed shapes. For all the cases, initial delaminations and cracks for the CAI models are accurately taken from the damage predictions of the impact models. A comparison of numerical results with experiments and existing results in literature of the simple straight fibre benchmark examples is illustrated to demonstrate the effectiveness of the current models for predicting the extent of impact damage and subsequent compression strength. For the case of VAT laminate, experimental data is not yet available. For this reason all the parameters (material

properties, panel size, layup, boundary conditions, etc.,) are exactly the same as the ones of the benchmark examples [23-24], except the fibre orientation variation in each layer. Here the use of validated numerical models is made to address the damage tolerance analysis of VAT laminates and to investigate how variation of fibre orientation affects performance in impact and compression after impact, which are two industry standard tests. This is one of the first studies in this area for variable angle tow laminates and it provides useful information for the understanding of the interaction between material orientation, matrix cracks and delaminations. Further work will develop experimental data for these cases, guided by initial analysis results, finally leading to full validation. Significant insight into the damage resistance and tolerance can still be gained from the analysis at this early stage despite the lack of available experimental results.

The paper is organized as follows. In Section 2, the definition of fibre path is given, where fibre path with linear fibre angle variation is considered. In Section 3, the modelling of low-velocity impact tests is performed, in which the presentation of the impact model along with numerical results and discussions is given in detail. Section 4 covers the modelling of compression after impact (CAI) tests, in which details of CAI model, numerical results and discussions are presented. A summary and conclusions are presented in Section 5.

## 2. Fibre path definition

Descriptions of fibre orientation variation for composite laminates that possess variable stiffness properties are introduced here. The simplest definition employs a unidirectional variation based on a linear function for the fibre orientation angle of the individual layers. It is assumed that the fibre angle of the reference fibre path varies linearly from the value $\theta_0$ at the centre of the panel to $\theta_1$ at a specified distance. This distance is often taken as a characteristic dimension of the panel. In the case of rectangular laminates this is generally half of the panel width, *a/2*, in the direction along which the linear variation takes place. Therefore, the orientation of a single curvilinear fibre path can be denoted using $\langle \theta_0 | \theta_1 \rangle$. Since a ply is made of fibres which are all oriented similarly to the reference fibre path, the description of the reference fibre path will also serve to describe the ply. A ‘‘±’’ sign in front of this term means that there are two adjacent layers with equal and opposite $\theta_0$ and $\theta_1$ angles.

The origin of the variation ($x_0$, $y_0$), is defined to be located at the centre of the plate (see Fig. 1). In this case, the reference curve is assumed to be anti-symmetric about the origin of the variation. The piecewise continuous functions which define the fibre path orientation can be determined in terms of $\theta_0$ and $\theta_1$:

$$\theta(x)=\begin{cases}\dfrac{2(\theta_0-\theta_1)}{a}x+\theta_0, & -a/2\le x\le 0\\ \dfrac{2(\theta_1-\theta_0)}{a}x+\theta_0, & 0\le x\le a/2\end{cases} \tag{1}$$

and the fibre path can be computed as:

$$y=\int_{-a/2}^{a/2}\tan\left[\frac{2(\theta_1-\theta_0)}{a}|x|+\theta_0\right]dx \tag{2}$$

In the present paper, the axis of fibre angle variation ($x$) is in the loading direction for CAI tests. Because of fibre variation, material properties in the finite element model are varied from element to element. In order to handle this issue, a code was written in Matlab to define material properties in VAT composite laminates. The code is linked to Abaqus/Explicit for modelling of VAT composite laminates and is validated through benchmark examples of VAT laminates [8].

## 3. Modelling of low-velocity impact tests

*3.1 Details of impact models*

The impact model of composite laminates to predict the damage induced by low-velocity impacts is presented in this section. Firstly, parameters defining the cohesive behaviour of the interface are identified by comparison of numerical results with experimental data [23]. Since experimental data and material properties are not available for VAT laminates, the same material properties from the straight fibre reference case [23] is used for the VAT laminate models. In the verification work, different features such as cohesive interface element model parameters, surface-based cohesive behaviour, mass scaling, material density, element size and meshing issues are also investigated in detail using Abaqus/Explicit [21]. As a benchmark for impact modelling of composite laminates an example from literature [23-24] was used.

We consider a $[0_3/90_3]_s$ laminated specimen (65 *mm* x 87.5 *mm* in size) simply supported by a steel plate having a rectangular opening 45 *mm* x 67.5 *mm* in size, and impacted by a 2.3 kg mass having a hemispherical indenter of 12.5 mm in diameter [23]. The $0_3$ and $90_3$ sublaminates are each modelled

through their thickness with two C3D8R reduced integration solid elements, while COH3D8 cohesive elements are inserted at the two interfaces between layers with different orientation (top $0^o/90^o$ interface and bottom $90^o/0^o$ interface). A thickness of 20 $\mu m$, which is maintained throughout the study, is assumed for the cohesive interface, laminate and interfacial properties are shown in Table 1. To simulate the initiation and growth of the major intralaminar tensile matrix crack, typically developing along the fibre direction in the lower block of layers of clustered cross-ply laminates [13], cohesive contacts (see Fig. 2) are used for the interaction between two crack surfaces assumed on the symmetry plane parallel to the $0^o$ direction. The cohesive properties of Table 1 are used for modelling both the tensile crack and delaminations. An element size of 0.5 *mm* by 0.5 *mm* (on the laminate plane) is used in the region of the damaged area for the laminate, while cohesive elements with the same size of 0.5 *mm* by 0.5 *mm* are used for the whole cohesive layer, the cohesive elements are attached to the laminate elements using *Tie Constraints* in Abaqus [21] (see Fig. 2) and the meshes are dissimilar. The fine mesh region on the laminate plane is 20 *mm* x 40 *mm*. The impactor was modelled as a rigid analytical surface associated with a pointwise mass. Two impact energies ($E$=2.1$J$ and $E$=6$J$) are simulated by imposing the the appropriate velocity to the impactor at the moment of contact, as computed from $v = \sqrt{\frac{2E}{m}}$, $E$ is the impact energy and $m$ is the mass of the impactor, the bottom support steel plate is a rigid body discretised with R3D4 rigid elements. The analyses were carried out on a parallel computing system of 8 CPUs with two 3.2 GHz Pentium *D* processors. Contact between the impactor and the laminate specimen is simulated by the general contact algorithm in Abaqus/Explicit [19] which uses a penalty enforcement contact method. This contact formulation is also applied between the different composite layers when the cohesive elements become fully damaged and are removed from the mesh. Friction with a coefficient of 0.3 is introduced between all the contacting surfaces.

*3.2 Straight fibre benchmark*

The model predictions are validated by comparison with experimental and numerical results from literature [23-24]. Figure 3 shows that a very good agreement is observed between experiments and predictions in both the peak force values and the impact durations for impact energy of 2.1$J$.

Figure 4 shows the magnified views of predicted results in terms of damage evolution and delamination size within the top interface $0^0/90^0$ and the lower interface $90^0/0^0$. Good agreement is also observed between simulated and experimental results of damage evolution and delamination size. Numerical analyses indicated that the initial damage, occurring at a load level about 1300 N, consists of a tensile matrix crack that developed within the bottom $0^0$ layer and quickly propagated towards the boundary of the sample. Following the formation of this crack, and in accordance with experimental evidence, the model predicts the onset of delamination on the lower $90^0/0^0$ interface and its growth with the characteristic two lobed shape elongated along the $0^0$ direction (Fig. 4a), this observation was found by Aoki, Suemasu and Ishikawa [27]. Delamination size obtained from the current simulation on the upper $0^0/90^0$ interface as shown in Fig. 4b also is a good agreement with that from [23-24] using the quadratic failure criterion for the onset of delamination [22]. However, it was reported [23-24] that if the quadratic failure criterion is used with the effect of out-of-plane compression in the damage onset criterion taken into account, which leads to the Hou criterion [28] for the onset of delamination, then a more accurate prediction at the upper $0^0/90^0$ interface is obtained which can better match experimental results.

Figure 6 shows a comparison between force-time curves obtained numerically and experimentally for the $[0_3/90_3]_s$ laminate with impact energy of 6*J*. As seen, a reasonable agreement was obtained between simulated and experimental results, however we can realize that a greater difference between these curves can be observed compared to the 2.1*J* case. Damage evolution and delamination size at the upper and lower interfaces are shown in Fig. 5, no experimental results are available for comparison.

3.3 *Variable Angle Tow (VAT) laminate*

A similar stacking sequence to straight fibre laminate and the same material properies are used in this section. Except for the variation of fiber direction in the plies, all boundary conditions, number of layers, mesh size and other parameters are the same as shown in Fig. 2 for the straight fibre laminate, $[0_3/90_3]_s$. A linear variation of the fiber orientation along the *x* coordinate is defined as in Eq. (1). The fibre paths defined in literature [8] are considered, the fibre path in the top three layers and the last three layers is denoted $\langle +45|0\rangle$, while the fibre path in the middle six layers is denoted $\langle -45|0\rangle$. A potential matrix-crack (coincident nodes joined by cohesive contact) is inserted in the bottom block of 3 layers, passing through the origin at centre of the plate. This tensile crack is assumed to lie along the fiber orientation.

The crack path is defined by Eq. (2) and was explicitly included in the mesh using a Matlab pre-processing script (see figure 7). Figures 6 to 9 show predicted results for variable stiffness laminate denoted $\left(\langle 45|0\rangle_3, \langle -45|0\rangle_3\right)_s$ with the impact energy of 6*J*, which is large enough to clearly observe damage evolution.

Figure 6 shows comparison of predicted force-time curve for the laminate $\left(\langle 45|0\rangle_3, \langle -45|0\rangle_3\right)_s$ and experimental force-time curves for the straight fibre laminate $[0_3/90_3]_s$, and its predicted force-time curve as well. It can be seen that although layups are notably different, the maximum impact load obtained for the variable stiffness laminate with the fiber path denoted as $\left(\langle 45|0\rangle_3, \langle -45|0\rangle_3\right)_s$ is not significantly different to that of the straight fibre laminate $[0_3/90_3]_s$. Figure 7 shows the mesh used for the VAT plies and cohesive elements at the inter-ply interface. The predicted results from the impact model of the VAT laminate $\left(\langle 45|0\rangle_3, \langle -45|0\rangle_3\right)_s$ in terms of damage evolution and crack propagation are presented in Figures 8-9. It is apparent that the effect of fibre orientation and the tensile crack on delamination shape and size is very significant. The delamination in both the upper interface and the lower interface tends to propagate along the fibre direction of the lower ply of the interface. However, the stability of the initial delamination and each delamination shape are quite different. The final delamination shape is affected by the existing matrix-cracks. The delamination adjacent to the bottom layer has an elongated shape along the tensile crack, being very sharp at the extremities of the crack. The effect of matrix cracks on the predicted delamination propagation is significant. Clearly, the impact model of the VAT composite laminate with such curvilinear paths of fibers and matrix-cracks explicitly defined is a good example for investigating the interaction between material orientation, matrix cracks and delaminations. The maximum dimensions of delamination in the upper interface of the VAT and the straight fibre laminate do not change very much (16.51 *mm* in Fig. 5 vs. 17.16 *mm* in Fig. 8), while those of delamination in the lower interface of the VAT and the straight fibre laminate are 58.28 *mm* and 31.85 *mm*, respectively. The total delamination area in the VAT laminate is 826 $mm^2$, greater than that of 448 $mm^2$ in the straight fibre laminate. It is apparent that more delamination damage is caused in the case of the VAT laminate $\left(\langle 45|0\rangle_3, \langle -45|0\rangle_3\right)_s$ in comparison with the delamination damage in the straight fibre laminate $[0_3/90_3]_s$.

## 4. Modelling of compression after impact tests

*4.1 Details of CAI model*

The CAI behaviour of the impacted VAT laminate $\left(\left\langle 45\,|\,0\right\rangle_3, \left\langle -45\,|\,0\right\rangle_3\right)_s$ and the impacted straight fibre laminate $[0_3/90_3]_s$ is studied in this section, the impacted laminates under the impact energy of 6J have the same dimensions 87.5 *mm* x 65 *mm* x 2.076 *mm*, its one quarter is as shown in Fig. 2. The CAI model for the post-impact compression behaviour prediction will accurately account for relevant details of the damage morphology of delaminations and cracks induced by low-velocity impacts from their impact models. A linearly increasing x direction compressive displacement is applied at $x = a/2$ with x=-a/2 held constant. The sides of the plate were simply supported at $y = \pm b/2$ and not constrained in-plane (see Fig. 10). Thus, the boundary conditions of the laminates are:

$$\begin{aligned} &u = w = 0 \text{ at } x = -a/2 \\ &u = u_o, w = 0 \text{ at } x = a/2 \\ &w = 0 \text{ along the line } y = \pm b/2 \text{ and } z = 0 \end{aligned} \tag{3}$$

The mechanical properties of the laminates and interfacial properties are shown in Table 1. The morphology of delaminations and cracks induced in the impact simulations is accurately taken as the starting point for damage in the CAI simulations. In the CAI model, delamination and crack propagation will also be considered.

Similarly to the impact model, C3D8R reduced integration solid elements are used for the laminates in the CAI model. Cohesive elements, COH3D8, with element size 0.5 *mm* by 0.5 *mm*, are inserted in selected regions of the two interfaces between layers of different orientation. This was only where un-failed cohesive elements from the impact analysis remained, representing no delaminations (see Fig. 8). Failed cohesive elements from the impact analysis, representing delaminations, are deleted for the CAI simulation and replaced by a contact formulation in Abaqus/Explicit [21]. The tensile crack (see Fig. 9) generated in the impact model is kept and still assumed to propagate along the fibre orientation. Cohesive contacts are used to simulate the crack propagation in the CAI models.

Two CAI analyses were performed as follows:

a) CAI simulations are performed for the impacted straight fibre laminate $[0_3/90_3]_s$ for the two cases: Firstly, the CAI model with the consideration of delamination and crack growth. In this case, initial delaminations and crack are accurately taken from the impact model (see Fig. 5). Secondly, the CAI model with the consideration of delamination growth and no tensile cracks, in which only delaminations are taken from the impact model. The purpose of this investigation is to answer open questions on what is the main reason for a significant reduction in the compressive strength of composite laminates that results from an impact, and on how the existence of cracks in the CAI model affects the deformed shape of composite panels. The CAI model of intact laminates (without any damage) will also be performed for these examples for comparisons.

b) CAI simulations are performed for the impacted VAT laminate $\left(\langle 45|0\rangle_3, \langle -45|0\rangle_3\right)_s$. In this CAI model, initial delaminations and cracks are taken from the impact model (see Figs. 8-9), delamination and crack growth are considered in the CAI model. The purpose of this investigation is to study how material orientation and matrix crack affect the evolution and size of damage when changing from straight fibers to curvilinear fibers in the laminate, the CAI model of intact laminates (without any damage) will also be performed for this example for comparison.

Since there are no examples of CAI testing or modelling were presented in Aymerich et al [23] for the straight fibre benchmark case against which to compare the current models (as was done for the impact case), an additional validation case was run. The result of Suemasu et al [25] was used for this validation. The laminate has dimensions 100 *mm* x 150 *mm* x 3.2 *mm*, boundary conditions are the same as shown in Eq. (3), the material of the laminate is quasi-isotropic carbon fibre reinforced plastic with $E_x = E_y = 57.5$ GPa, $E_z = 8.87$ GPa, $\nu_{xy} = 0.32$, $\nu_{xz} = \nu_{yz} = 0.34$, $G_{xy} = 21.78$ GPa, and $G_{xz} = G_{yz} = 4.605$ GPa. Three artificial delaminations with a diameter of 40 *mm* and equally-spaced in the thickness direction were inserted at the centre of the laminate (see [25], case 3D40 for more details). No matrix crack is considered in this example and good agreement was achieved (see Fig. 10).

*4.2 CAI models of straight fibre laminates*

Figure 11 shows the force-displacement curves for the CAI simulation of the impacted straight fibre laminate $[0_3/90_3]_s$ for the two cases: firstly, the CAI model with the consideration of delamination and crack growth (see the green line: *0-C1-C2-C3-C4* in Fig. 11), in this case, initial delaminations and crack are accurately taken from the impact model. Secondly, the CAI model with the consideration of delamination growth and no tensile cracks (see blue line: 0-*UC1-UC2-UC3-UC4* in Fig. 11) as per the benchmark example. In this case, only delaminations are taken from the impact model (see Fig. 5). It can be seen that delaminations in the CAI model without matrix-cracks started at later time, $t$ = 0.390 seconds (point *UC1*), than delamination starts in the CAI model with the tensile crack, $t$ = 0.345 seconds (point *C1*). It seems however that the tensile crack does not affect the maximum compressive load ($P$= 26.043 *KN* at *C*1 and $P$= 27.046 *KN* at *UC1*) too strongly. The compressive load obtained from both these CAI models is lower than that of the CAI model of the intact straight fibre laminate (without any damage consideration), this is as expected.

The evolution of damage (delamination and crack) and their size at different times for the laminate with delamination and crack growth is presented in Fig. 12. As observed, delaminations started in the lower interface (at the point *C1*) and the load increased by a small amount to the point *C2* and then dropped sharply (see Fig. 12) after a significant delamination event happened (see Fig. 12 from *C2* to *C3*). Figure 13 shows the delamination area as a function of applied displacement for the straight fibre laminate with the consideration of dalamination and crack growth, it is seen that the delamination area in the upper interface is constant and that in the lower interface it is increasing with the applied displacement, thus delamination propagated in the lower interface only, not in the upper interface. This observation is also observed in the straight fibre laminate with delamination growth and no cracks.

The failure of damaged laminates under uniaxial compression load is caused by local buckling of the sublaminates originated in the impact. Delamination propagated mainly perpendicularly to the loading direction (see Fig. 12), this trend has been reported in literature [10, 29].

*4.3 CAI models of VAT laminates*

Figure 14 shows the force-displacement curve (*0-P1-P2-P3-P4*) of the VAT laminate $\left(\langle 45\,|\,0\rangle_3, \langle -45\,|\,0\rangle_3\right)_s$ with consideration of delamination and crack growth. The evolution of delaminations and matrix crack at different points is presented in Figure 15 while the relationship

between the delamination area and the applied displacement is shown in Figure 16. It can be observed that delamination starts at point *P1* ($u$ =0.33 *mm*, $t$ =0.375 seconds) in the lower interface, the load increases by a small amount from point *P1* to point *P2* ($u$ =0.471 *mm*, $t$ =0.44 seconds) where the maximum load of 23.572 *KN* is obtained. After the point *P2*, the load dropped sharply (*P2-P3*) after a significant delamination event occurred in the upper interface as shown in Fig. 15 (see delamination evolution from *P2-P3* at the upper interface) and in Fig. 16 (see the gradient of delamination area in the section $\Delta u_1$ ). After the first significant damage event happened in the upper interface, the load was nearly constant between points *P3 and P4*, because no significant damage event occurred and thus delamination area was constant with respect the applied displacement (see Fig. 16). The second significant damage event happened in the lower interface as shown in Fig. 15, and thus the second big drop of load was obtained (see *P4-P5* in Fig. 14).

Here, as with the straight fibre laminate, delaminations in both the upper and lower interfaces propagate mainly perpendicularly to the loading direction; this observation was also made by Soutis and Curtis [10] and Sanchez-Saez et al [29]. It is also observed that delaminations propagated in the lower interface only for the straight fibre laminate (see Fig. 12) but propagated in both the upper interface and the lower interface for the VAT laminate (see Fig. 14), this means that for the laminates with the same stacking sequence, but when material orientations in sublaminate blocks of the laminates varied, delaminations can occur at different interfaces through the thickness. This can be explained as follows: the delaminations are generated mainly by the differences between the bending stiffness of the adjacent plies, and when the fibre path is changed from straight to curvilinear, the bending stiffness of sublaminates is also changed and the profile and size of delaminations at interfaces induced from impacts is changed, unstable damage growth is obtained by CAI due to a buckling mechanism in the delaminated area, and thus the delamination sequence happening in interfaces will be different.

Figure 17 presents deformed shapes of the VAT laminate with damage growth at some specific instants. It is apparent that when the consideration of damage growth is taken into account in VAT laminates, its CAI behaviour is very complex. At the time of delamination start (*P1*), the bottom sublaminate contained a tensile crack and become the weakest one among the sublaminates; moreover the delamination size induced from the impact at the lower interface was larger. The deformed shape remained the same with a

larger magnitude of deformation until point *P2* at which the maximum load is obtained. It is worth noting that when the laminate contained cracks, the deformed shape at the instants *P1* and *P2* is in the opposite direction of that of laminates without cracks, this finding is consistent with the straight fibre laminate with cracks. When the first significant damage event occurred in the upper interface, the top sublaminate started buckling locally (see *P4* in Fig. 16), while the laminate still continued to buckle globally in the bottom sublaminate. At point *P5*, the second significant delamination event has just happened in the lower interface and the tensile crack has completely propagated to the fixed two edges.

The force-displacement curves for the straight fibre and VAT laminates with damage growth (see Fig. 11 and Fig. 14) lie below those of their intact laminates (without damage), as expected. Failure of damaged laminates under uniaxially compressive load is caused by local buckling of the sublaminates, which is induced from the impact. The bending stiffness of the sublaminates is lower than that of a non-impacted laminate, so they buckle locally, and failure occurs under a lower load than in an undamaged laminate.

In all simulations the fibre direction compressive stress was monitored. At no time did it exceed a maximum of 1257MPa and 1190 MPa for the straight fibre laminate and the VAT laminate, respectively, which is well below fibre compression strengths of typical carbon/epoxy laminates. Therefore although the models presented did not explicitly include a progressive fibre failure model, it is shown that this is not necessary and that the delamination failures predicted are the dominant failure mode.

## 5. Conclusions

This paper has presented a study on the effect of fibre orientations on the impact and post impact compression behaviour of straight fibre and VAT laminates. This was achieved using an explicit finite element analysis, in which bilinear cohesive law-based interface elements and cohesive contacts were used to model the delamination and crack growth. Impact and CAI simulations were performed to enhance the understanding of the interaction between material orientation, matrix cracks and delaminations. Some remarks on this work can be summarized as follows.

(1). The main reason for the significant reduction in the compressive strength of the damaged laminates induced by impacts is the occurrence of significant delamination events.

(2). In the impact models, all of the delaminations propagated in the fiber direction of the layer below their interfaces. However, the stability of the initial delamination and each delamination shape were quite different, guided by adjacent matrix cracks.

(3). In the CAI models, delaminations propagated perpendicularly to the loading direction, the propagation being less in the loading direction. Matrix-cracks do not have a significant effect on the evolution of delamination, but the existence of cracks originating from the impact plays an important role in determining the sublaminate buckling mode.

(4). Material orientation plays an important role on the evolution of delaminations in both the impact and CAI simulations. If the fibre path is changed from straight fiber to curvilinear fiber, damage growth obtained by CAI due to a buckling mechanism in the delaminated area is also changed.

Future work will investigate VAT laminates with more complex layups and hence more complex damage-fibre orientation interactions. Results will also be compared directly with experimental data when available.


### Acknowledgements

The authors wish to acknowledge EPSRC, Airbus and GKN for supporting this research under the ABBSTRACT2 project. The authors would also like to thank Professor Francesco Aymerich of the University of Caligari and Professor Hiroshi Suemasu of Sophia University for their help in supplying experimental data and helpful discussions.


**References:**


1. Renton WJ, Olcott D, Roeseler W, Batzer R, Baron W, Velicki A . Future of Flight Vehicle Structures (2000-2023). Journal of Aircraft 2004; 41(5):986-997.
2. Guy Norris. NASA's push toward carbon-neutral-airliners, the Aviation Week and Space Technology, February 7, 2012. URL: http://www.aviationweek.com/aw/generic/story_generic.jsp?channel=awst&id=news/awst/2012/02/06/AW_02_06_2012_p69-418462.xml&headline=null&prev=10

3. Kim BC, Potter K, Weaver PM. Continuous tow shearing for manufacturing variable angle tow composites. Composites: Part A 2012, doi: 10.1016/j.compositesa.2012.02.024.
4. Weaver PM, Potter KD, Hazra K, Saverymuthapulle, MAR, Hawthorne MT. Buckling of variable angle tow plates: From concept to experiment. 50th AIAA/ASME/ASCE/AHS/ASC Structures, Structural Dynamics and Materials Conference, 2009.
5. Wu Z, Raju G, Weaver PM. Buckling analysis of VAT plate using energy method. 53rd AIAA/ASME Structures, Structural Dynamics and Materials Conference, Hawaii, April 2012.
6. Raju G, Wu Z, Kim BC, Weaver PM. Prebuckling and buckling analysis of variable angle tow plates with general boundary conditions. Composite Structures 2012, 94: 2961–2970.
7. Hyer M, Charette R. Use of curvilinear fiber format in composite structure design. AIAA Journal 1991; 29(6):1011-1015.
8. Gurdal Z, Olmedo R. In-Plane Response of Laminates with Spatially Varying Fiber Orientations: Variable Stiffness Concept. AIAA Journal 1993; 31(4): 751-758.
9. Tatting, BF, Gurdal Z. Design and manufacture of elastically tailored tow placed plates. NASA/CR 2002- 211919, 2002: 1-14.
10. Soutis C, Curtis PT. Prediction of the prediction of the post-impact compressive strength of CFRP laminated composites. Composites Science and Technology 1996; 56: 677-684.
11. Davies GAO, Hitchings D, Besant T, Clarke A, Morgan C. Compression after impact strength of composite sandwich panels. Composite Structures 2004; 63:1–9.
12. De Freitas M, Reis L. Failure mechanisms on composite specimens subjected compression after impact. Composite Structures 1998; 42: 365-373.
13. Abrate S. Impact on composite structures. Cambridge University Press, 1998.
14. Lammerant L, Verpoest I. Modeling of the interaction between matrix cracks and delaminations during ompact of composites plates. Composites Science and Technology 1996; 56: 1171-1178.
15. Salpekar SA, O'Brien TK, Shivakumar KN. Analysis of local delaminations caused by angle ply matrix cracks. Journal of Composite Materials 1996;30(4):418–40.
16. Moura MFSF, Goncalves JPM. Modelling the interaction between matrix cracking and delamination in carbon–epoxy laminates under low velocity impact. Composites Science and Technology 2004; 64: 1021–1027.

17. Ladeveze P, Lubineau G, Marsal D. Towards a bridge between the micro- and mesomechanics of delamination for laminated composites. Composites Science and Technology 2006; 66(6):698–712.
18. Hallett SR, Jiang W, Khan B, Wisnom MR. Modelling the interaction between matrix cracks and delamination damage in scaled quasi-isotropic specimens. Composites Science and Technology 2008; 68: 80–89.
19. Lopes C, Gurdal Z, Camanho, P. Variable-stiffness composite panels: Buckling and first-ply failure improvements over straight-fibre laminates. Computers and Structures 2008; 86: 897–907
20. Lopes CS, Camanho PP, Gurdal Z, Tatting BF. Progressive failure analysis of tow-placed, variable-stiffness composite panels. International Journal of Solids and Structures 2007; 44: 8493–8516.
21. Simulia Corp. Abaqus Theory Manual, Version 6.9-EF., Providence, RI, USA; 2009.
22. Harper P, Hallett SR. Cohesive zone length in numerical simulations of composite delamination. Engineering Fracture Mechanics 2008; 75(16): 4774-4792.
23. Aymerich F, Dore F, Priolo P. Prediction of impact-induced delamination in cross-ply composite laminates using cohesive interface elements. Composites Science and Technology 2008; 68: 2383–2390.
24. Aymerich F, Dore F, Priolo P. Simulation of multiple delaminations in impacted cross-ply laminates using a finite element model based on cohesive interface elements. Composites Science and Technology 2009; 69: 699–1709.
25. Suemasu H, Sasaki W, Ishikawa T, Aoki Y. A numerical study on compressive behavior of composite plates with multiple circular delaminations considering delamination propagation. Composites Science and Technology 2008; 68: 2562–2567.
26. Moura MFSF, Goncalves JPM, Marques AT, Castro PMST. Modeling compression failure after low velocity impact on laminated composites using interface elements. Journal of Composite Materials 1997; 31(15): 1462-1479.
27. Aoki Y, Suemasu H, Ishikawa T. Damage propagation in CFRP laminates subjected to low velocity impact and static indentation. Advanced Composite Materials 2007; 16 (1): 45–61.
28. Hou JP, Petrinic N, Ruiz C. A delamination criterion for laminated composites under low-velocity impact. Composites Science and Technology 2001; 61: 2069–2074.
29. Sanchez-Saez S, Barbero E, Zaera R, Navarro C. Compression after impact of thin composite laminates. Composites Science and Technology 2005; 65: 1911–1919.

## Figures

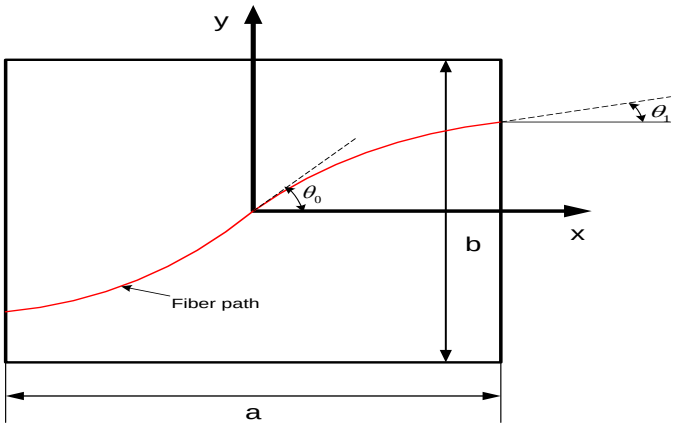


Fig. 1 Reference path definition of a variable layer.

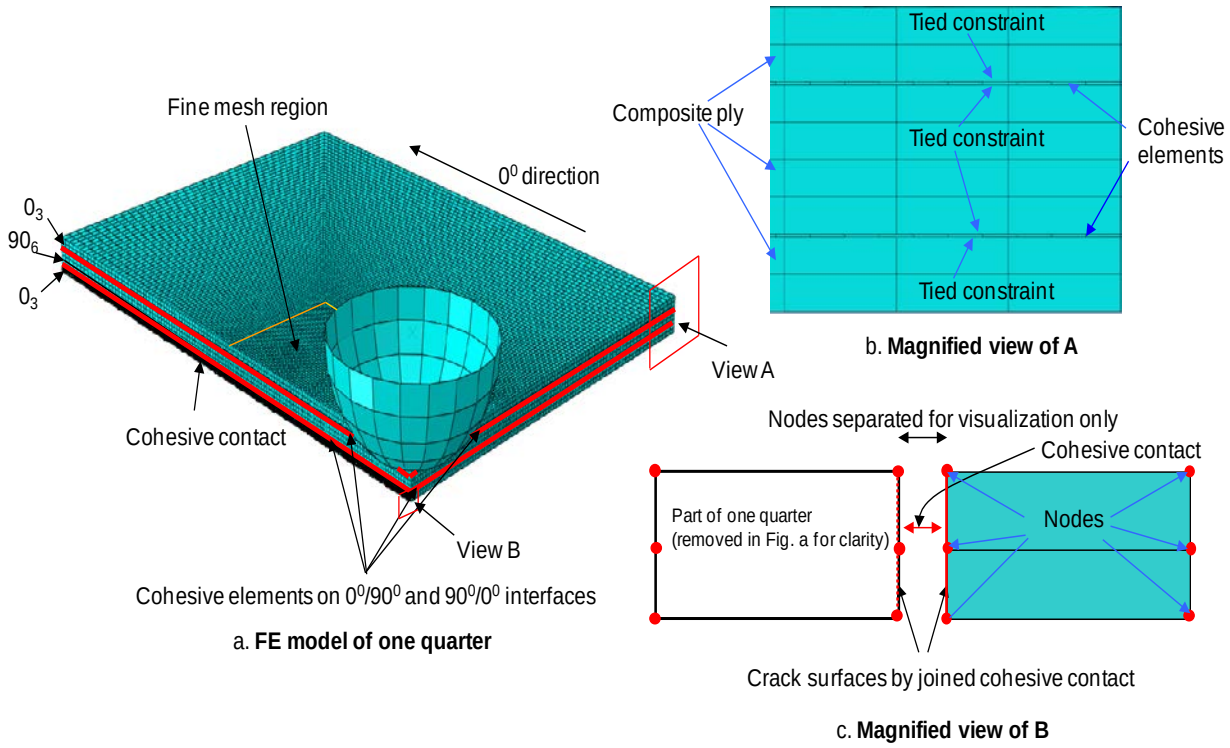


Fig. 2 Straight fibre FE model showing; a) Only one quarter of the full $[0_3/90_3]_s$ plate modelled, with cohesive elements for delamination at interfaces and cohesive contacts for tensile cracks; b) Magnified view of region A showing mesh in cohesive element layer and plies; c) Magnified view of region B showing details of tensile crack in the bottom layer using coincident nodes with cohesive contact.

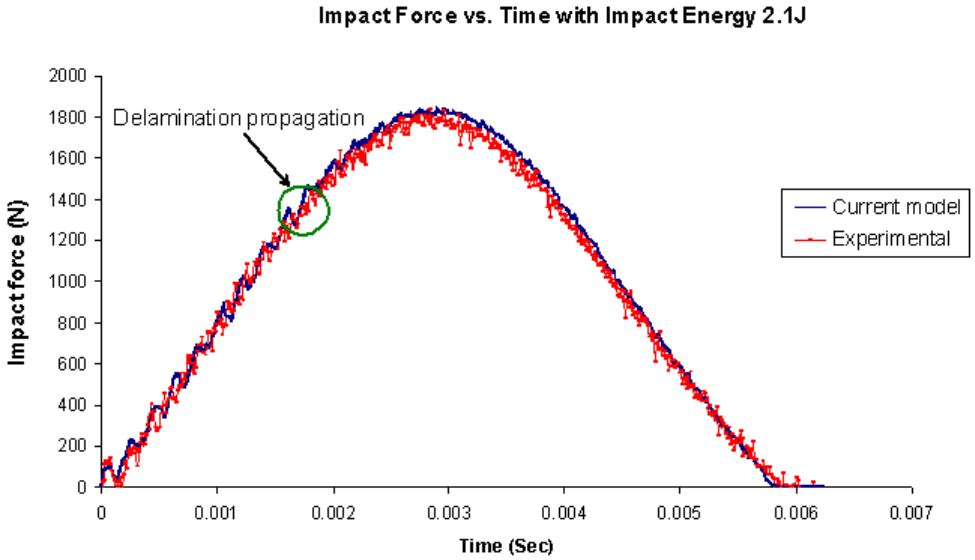


Fig. 3 Comparison between predicted and experimental force–time curves for the laminate $[0_3/90_3]_s$ with impact energy of 2.1*J*. Delamination propagation happens at 1.78 *msec* after contact takes place.

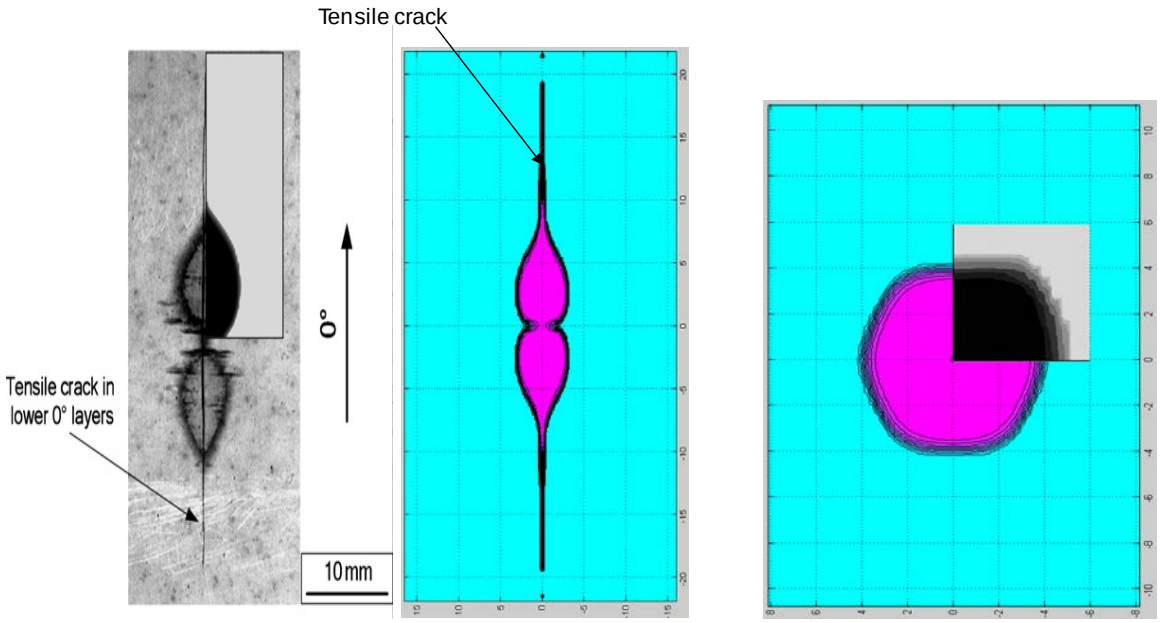


a. Lower $90^0/0^0$ interface b. Upper $0^0/90^0$ interface

Fig. 4 Comparison between delamination and damage of the current model with impact energy of 2.1*J* and experiment by X-radiography, along with predicted results in [21].

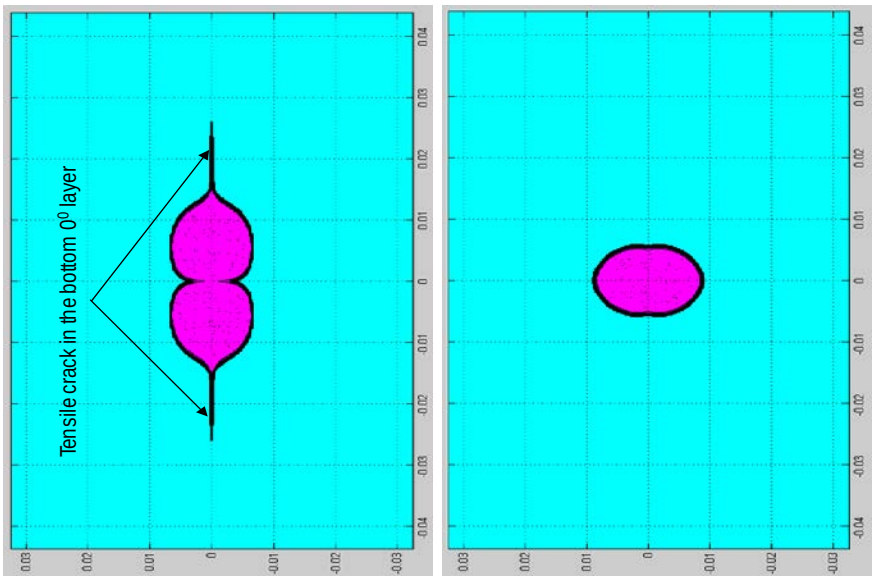


a. Lower $90^0/0^0$ interface b. Upper $0^0/90^0$ interface

Fig. 5 Delamination areas predicted by the impact model for the laminate $[0_3/90_3]_s$ with impact energy of 6 *J*.

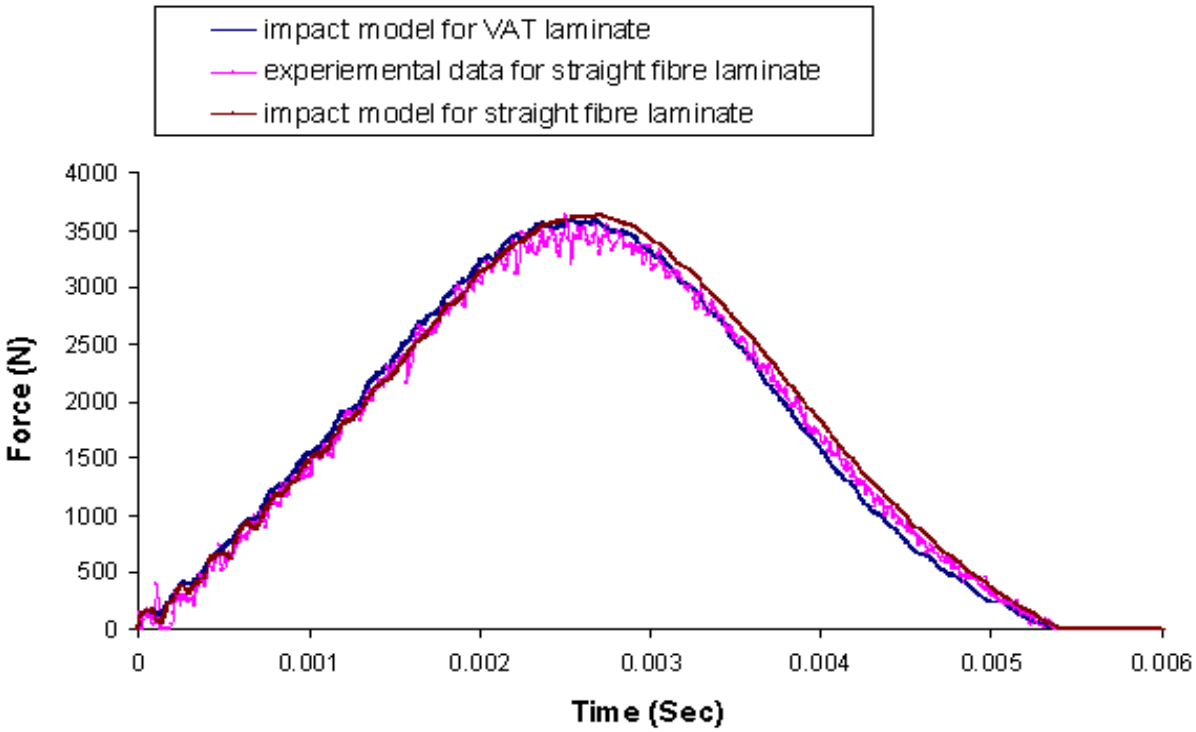


Fig. 6 Comparison between predicted force–time curve of the VAT laminate $\left(\langle 45|0\rangle_3, \langle -45|0\rangle_3\right)_s$ and the predicted and experimental force-time curves of the laminate $[0_3/90_3]_s$ with impact energy of 6*J*..

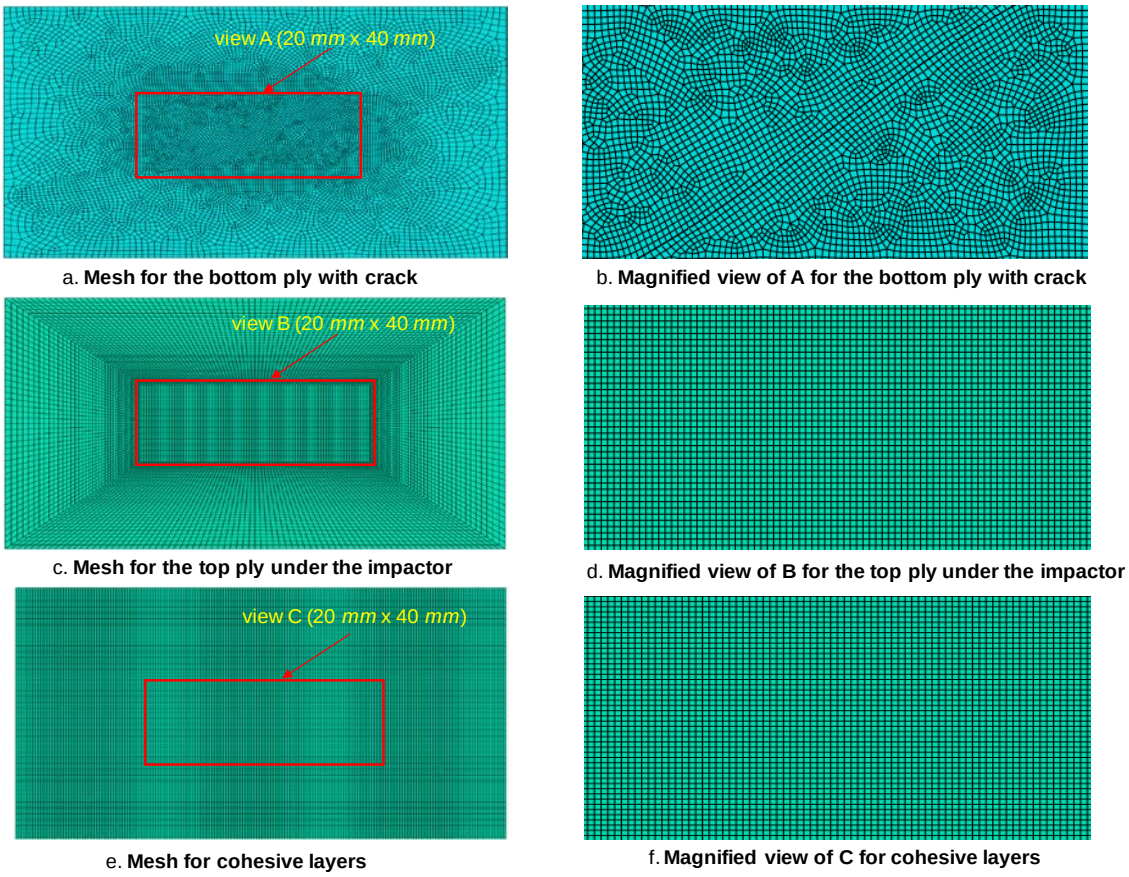


Fig. 7 Mesh for VAT modelling; a) The bottom ply with crack; b) Magnified view of region A; c) The top ply under the impactor; d) Magnified view of B; e) Cohesive layers; f) Magnified view of C.

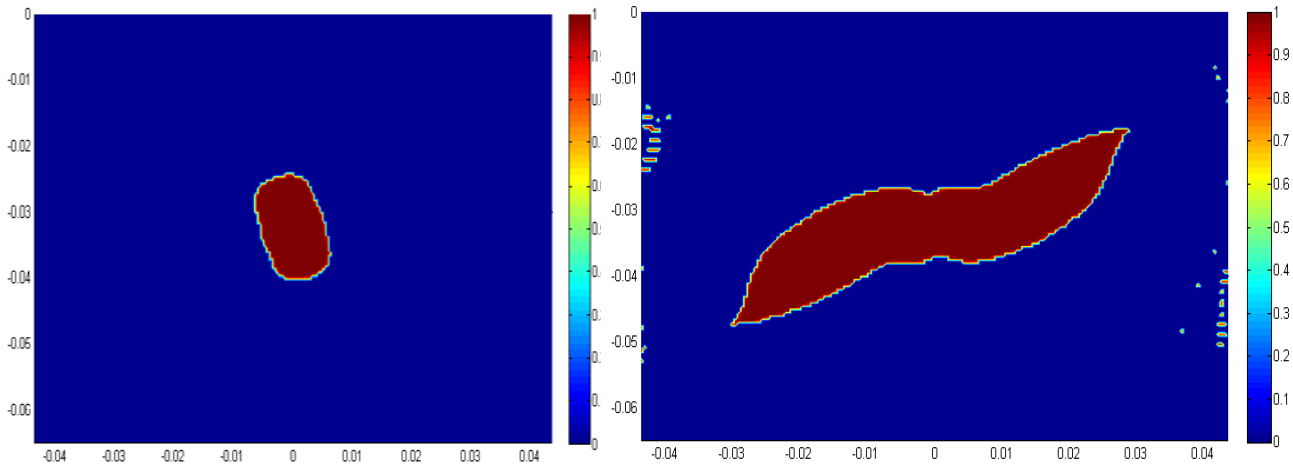

a. Upper interface b. Lower interface

Fig. 8 Delamination areas predicted by the current impact model for the laminate $\left(\langle 45\,|\,0\rangle_3, \langle -45\,|\,0\rangle_3\right)_s$ with impact energy of 6*J*.

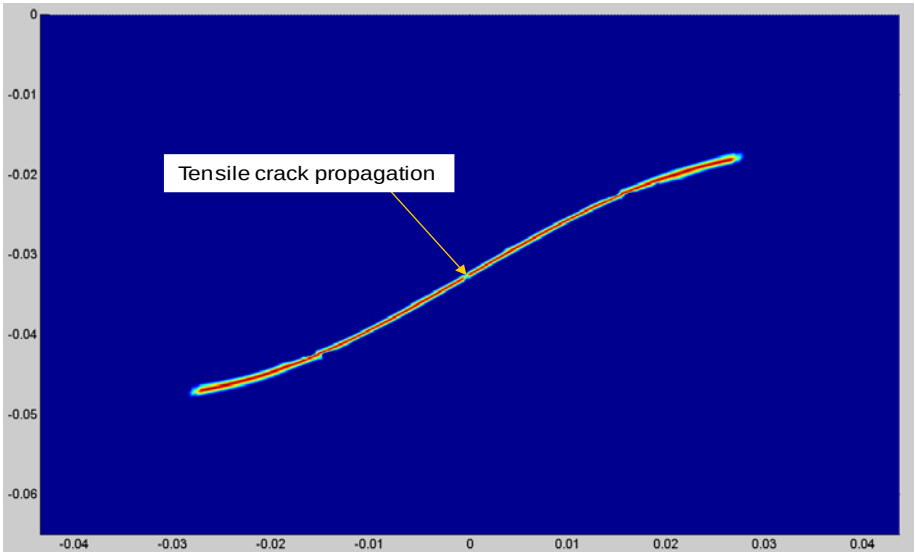


Fig. 9 Tensile crack propagation predicted by the current impact model for the laminate $\left(\langle 45\,|\,0\rangle_3, \langle -45\,|\,0\rangle_3\right)_s$ with impact energy of 6*J*.

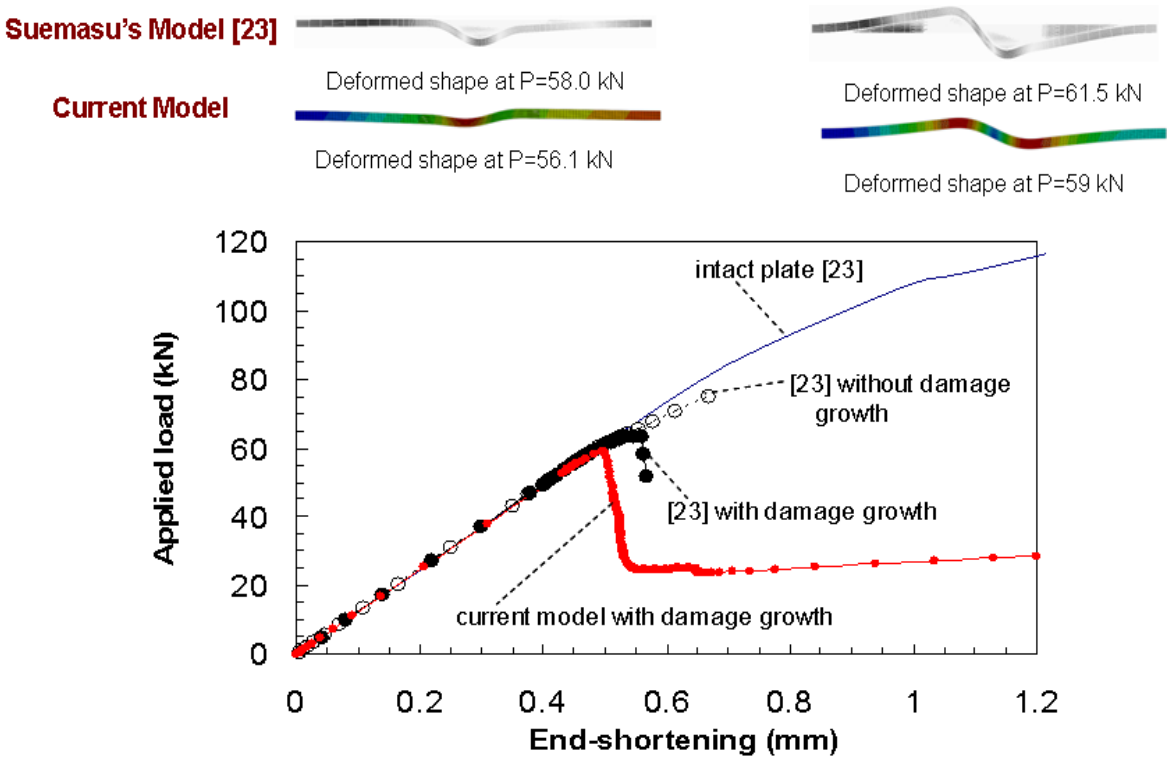


Fig. 10 Verification of the current model with a benchmark example [23] for three circular delaminations (3D40) for a laminate 100 *mm* x 150 *mm* x 3.2 *mm* without matrix-cracks

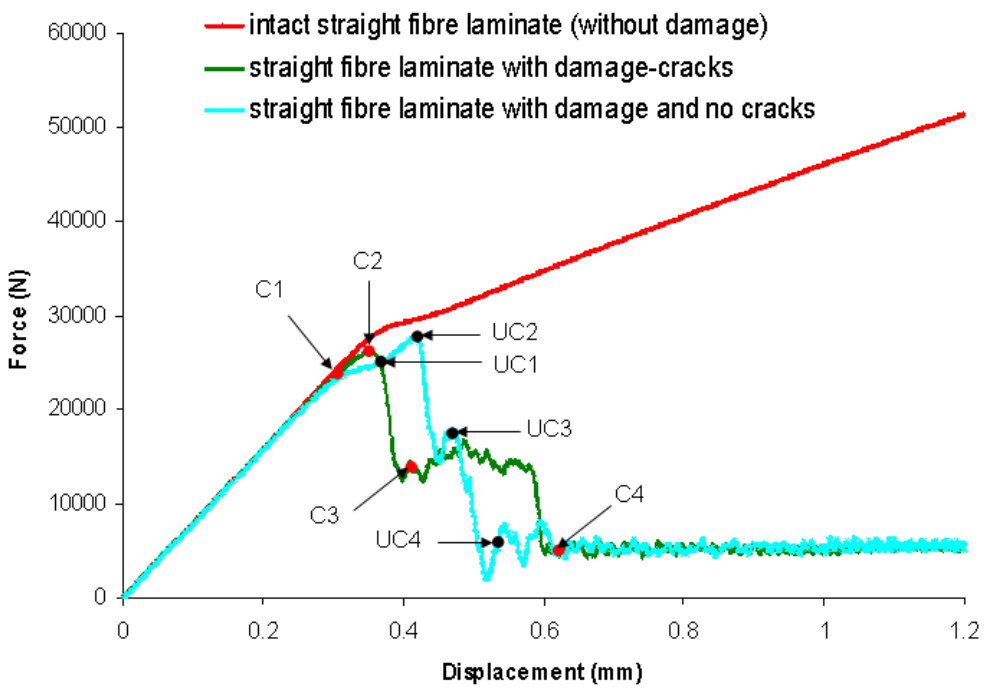


Fig. 11 Horizontal force-displacement curves of the laminate $[0_3/90_3]_s$ with damage and crack, with damage and no crack, and without damage.

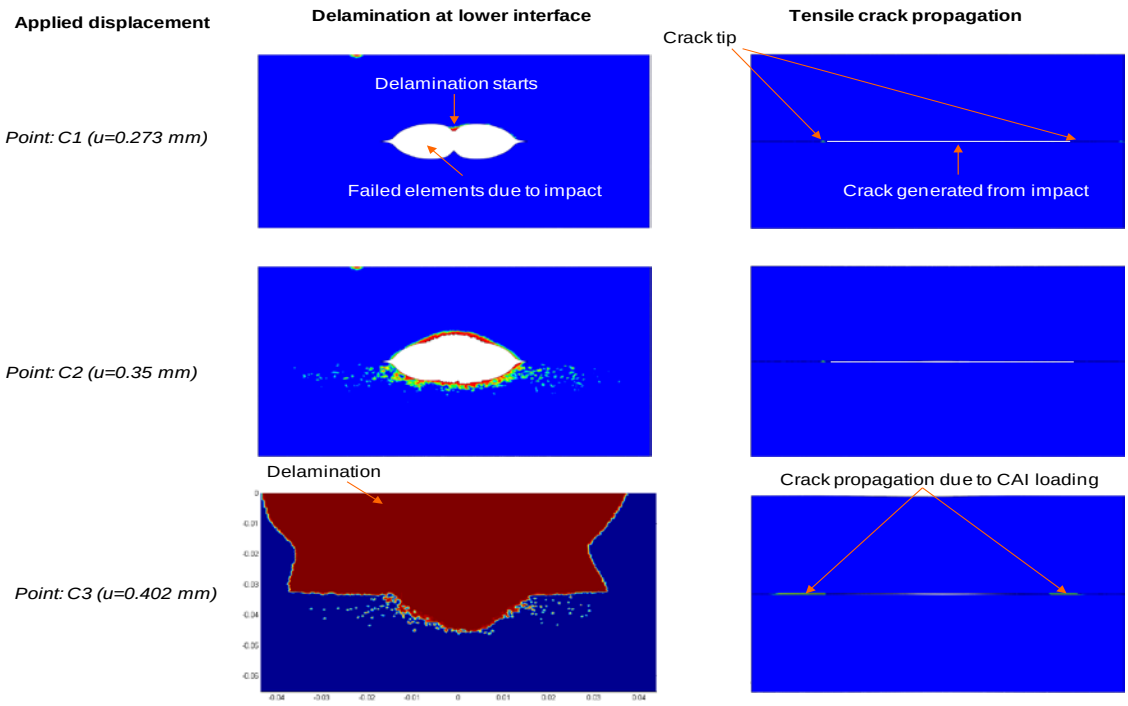


Fig. 12 Delamination and crack growth of the laminate $[0_3/90_3]_s$ with consideration of delamination and crack propagation in the laminate.

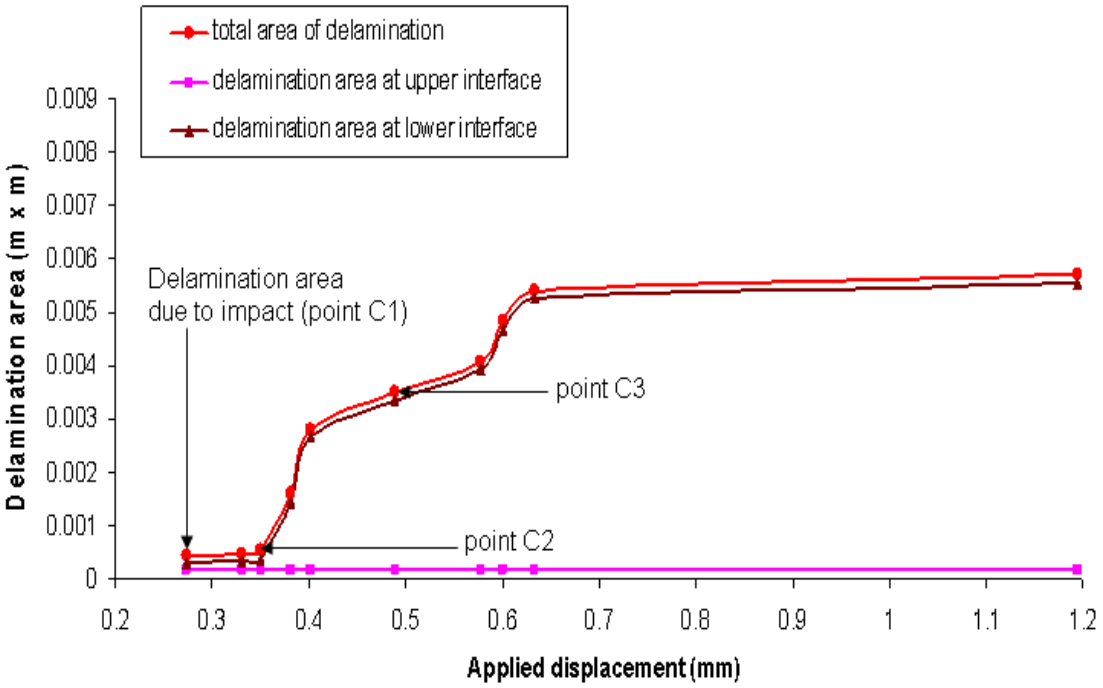


Fig. 13 Delamination area as a function of applied displacement for the laminate $[0_3/90_3]_s$ with consideration of delamination and crack propagation .

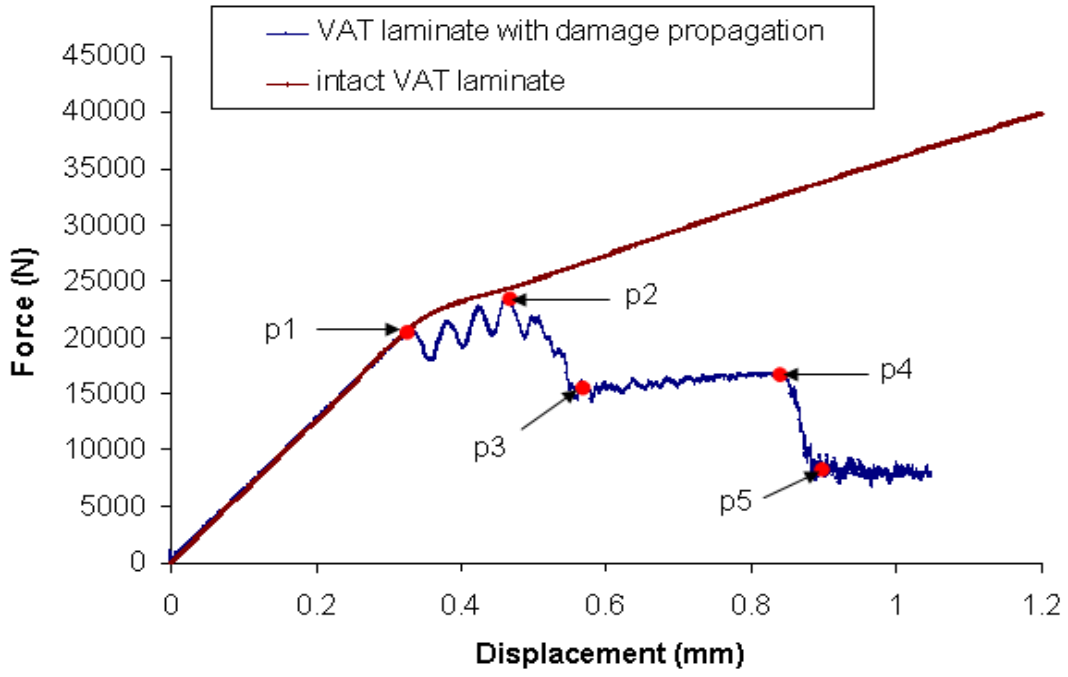


Fig. 14 Horizontal force-displacement curves of the VAT laminate $\left(\langle 45\,|\,0\rangle_3, \langle -45\,|\,0\rangle_3\right)_s$ with damage and crack, and without any damage.

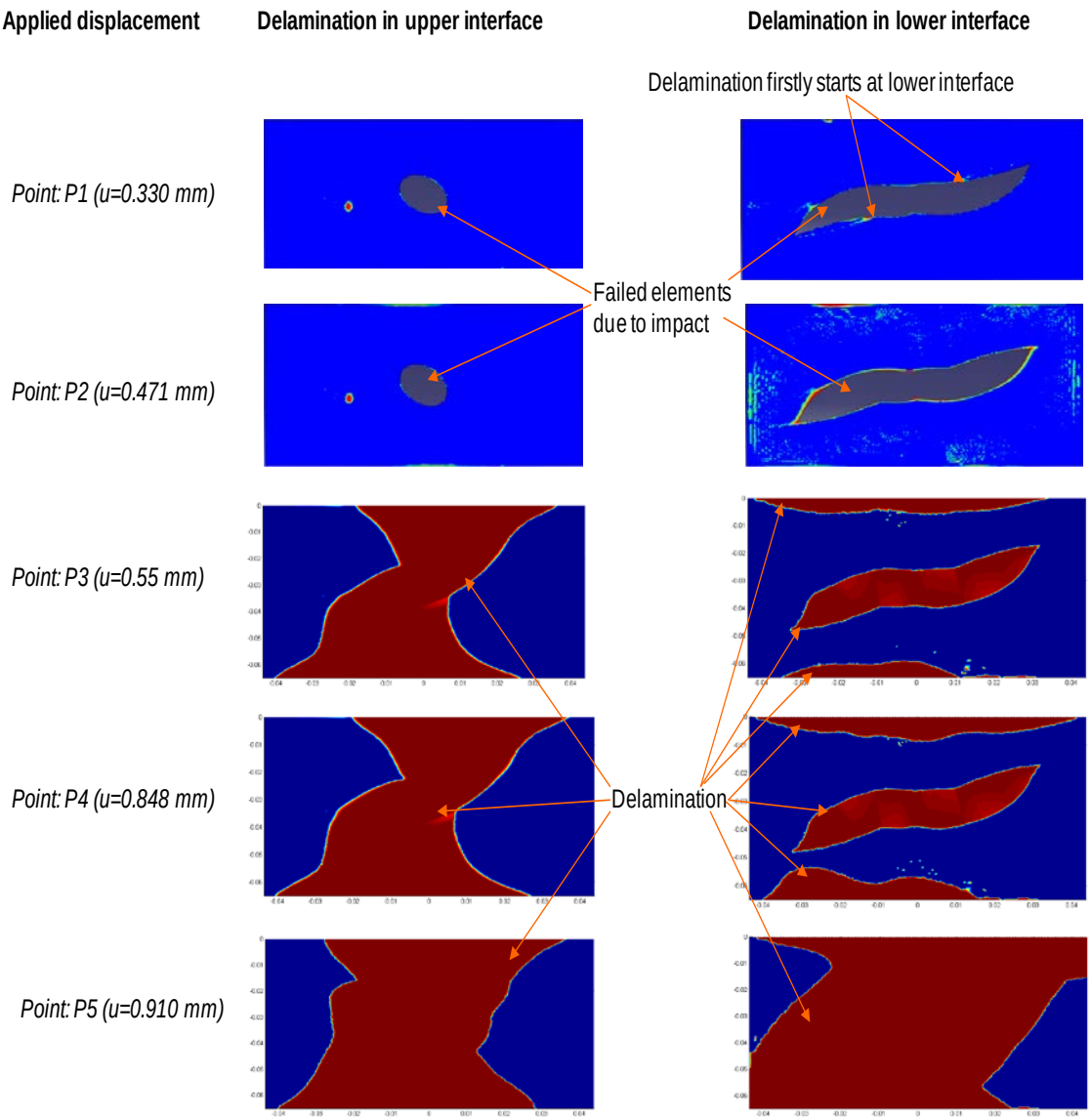


Fig. 15 Delamination growth of the VAT laminate $\left(\langle 45|0\rangle_3, \langle -45|0\rangle_3\right)_s$ with consideration of delamination and crack propagation.

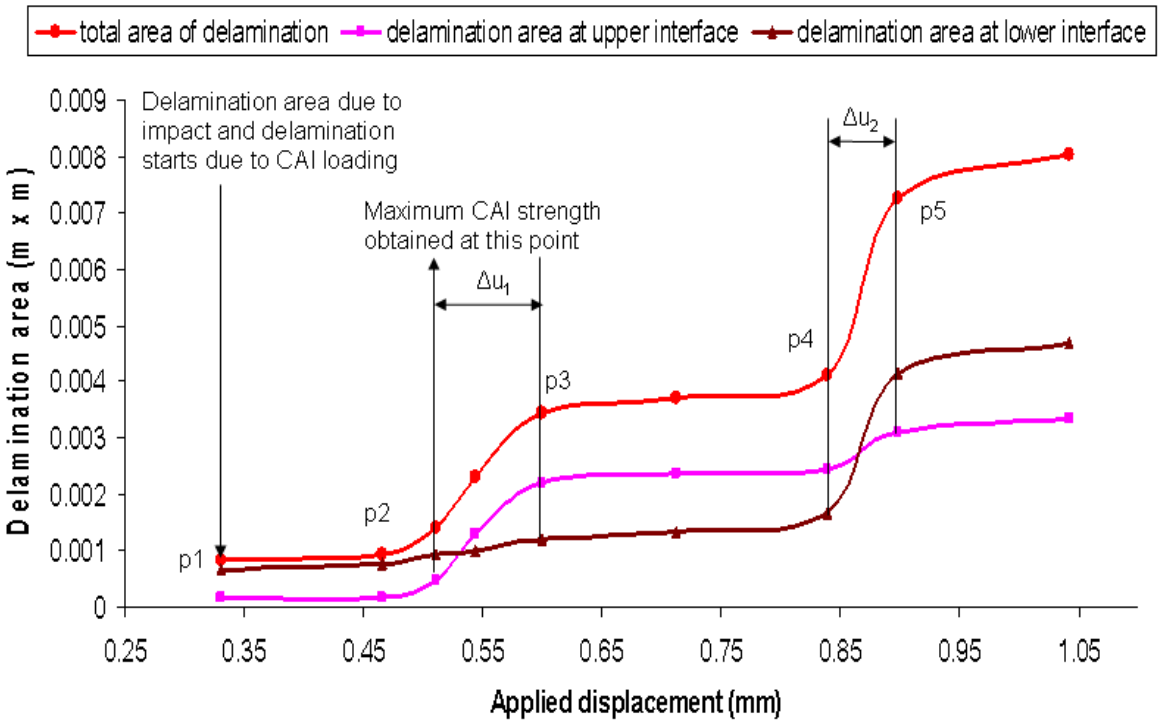


Fig. 16 Delamination area as a function of applied displacement for the VAT laminate $\left(\langle 45\,|\,0\rangle_3, \langle -45\,|\,0\rangle_3\right)_s$ with consideration of delamination and crack propagation.

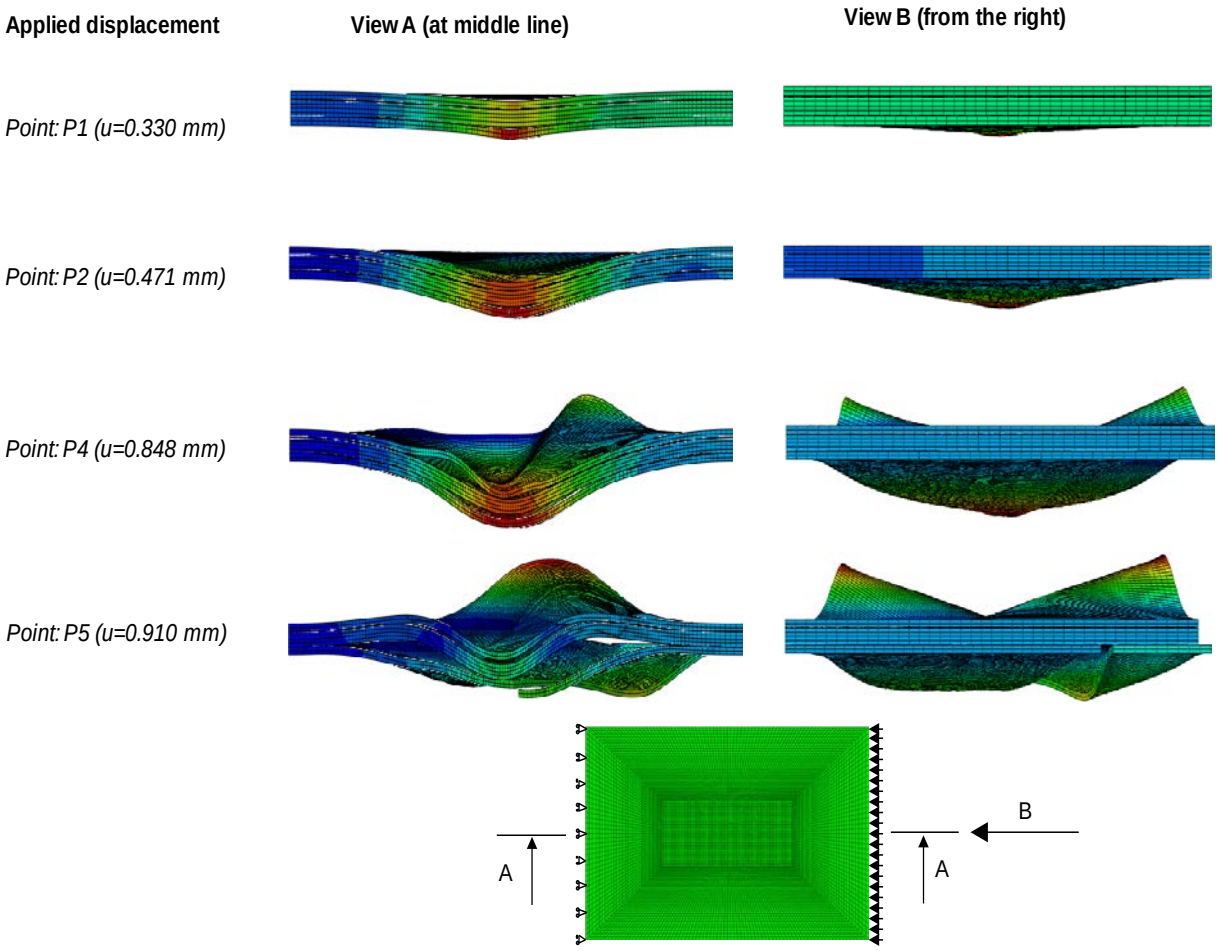


Fig. 17 Deformed shapes at different applied displacements of the VAT laminate $\left(\langle 45|0\rangle_3, \langle -45|0\rangle_3\right)_s$ with consideration of delamination propagation and without cracks.

Delamination start at t = 0.375 sec (u=0.33*mm*) in the lower interface.

## Tables

**Table 1** Laminate and cohesive properties used in the simulation [23].

| Laminate properties | | Cohesive properties | |
|---|---|---|---|
| $E_{11}$ (GPa) | 93.7 | $G_{IC}$ (J/m$^2$) | 520 |
| $E_{11} = E_{33}$ (GPa) | 7.45 | $G_{IIC} = G_{IIIC}$ (J/m$^2$) | 970 |
| $G_{12} = G_{23} = G_{13}$ (GPa) | 3.97 | $N$ (MPa) | 30 |
| $\nu_{12} = \nu_{23} = \nu_{13}$ | 0.261 | $S$=$T$ (MPa) | 80 |
| | | $k_{\mathrm{I}}$ (GPa/mm) | 120 |
| | | $k_{\mathrm{II}} = k_{\mathrm{III}}$ (GPa/mm) | 43 |